Vibration control of plates through a periodic array of shunted piezoelectric patches with negative capacitance circuits

F. Tateo[a], B.S. Beck[b], M. Collet[c], M. Ouisse[a], K.A. Cunefare[d], M.N. Ichchou[c]

[a]Femto-st, 26 rue de l'Epitaphe, 25000 Besançon;
[b]National Institute of Aerospace,100 Exploration Way, Hampton, VA 23666;
[c]École Centrale de Lyon, 36 avenue Guy de Collongue, 69134 Écully;
[d]Georgia Institute of Technology, North Avenue, Atlanta, GA 30332.

ABSTRACT

A two-dimensional array of piezoelectric transducer (PZT) shunted on negative capacitance circuit is designed and applied to achieve broadband vibration reduction of a flexible plate over tunable frequency bands. Each surface-bonded patch is connected to a single independent negative capacitance synthetic circuit.
A finite element-based design methodology is used to predict and optimize the attenuation properties of the smart structure. The predictions are then experimentally validated by measuring the harmonic response of the plate and evaluating some derived quantity such as the loss factor and the kinetic energy ratio. The validated model is finally used to explore different configurations with the aim of defining some useful design criteria.

Keywords: Metacomposites, Semi-active control, Negative capacitance circuit, Piezoelectricity.

1. INTRODUCTION

Shunted piezoelectric patches is a promising control technique for vibration suppression of flexible structures. The technique was first introduced by Forward[1] who used piezoelectric elements with active feedback circuits to significantly reduce the mechanical response of a membrane mirror. Contrary to active control, the only external element to be used is a passive electrical network that is directly connected to the electrodes of the piezoelectric device.
With this approach, the sensing element is not needed and the use of a passive network guarantees the stability of the coupled system. From the theoretical point of view the first analytical formulation of such passive shunt networks was provided by Hagood.[2] According to its interpretation the piezoelectric patch shunted through a resistive inductive circuit acts as a tuned mass damper adjusted at the resonance frequency of the circuit.
Since then, more complex shunting circuits have been investigated to extend the control system's effectiveness over broader frequency bands. For example, a multi-mode technique has been proposed by Wu[3] who employed a series of blocking, inductive-capacitive circuits in parallel with an RL shunt circuit designed to attenuate a specific resonance frequency. More recently, the idea of distributed vibration absorbers was introduced. For example it worth to mention the method based on an array of independently-shunted piezoelectric patches distributed over the whole structure. This results in a periodic configuration, where equivalent sources of mechanical impedance mismatch are introduced through proper tuning of the shunting circuits. The selection of this configuration is driven by the unique properties of broadband wave attenuation of periodic structures.
The propagation of waves in smart periodic rods and axisymmetric shells was studied by Thorp[5] who used RL piezoelectric shunts to passively control the vibration field. Recently Spadoni[6] extended the concept to flat plates demonstrating that the width and location of stop bands in the frequency domain can be shaped through the tunable characteristics of periodic RL shunts.
These techniques exploit the energy exchange mechanism established between the controlled structure and a resonating element to control its dynamic behavior. The effectiveness of this control strategy depends on the accurate knowledge of the modes of the controlled structures, for small variation of the tuning parameter of the external circuit a degradation in performance is usually observed. Moreover the RL control strategy suffer from another limitation, namely the impossibility to control the structure over a wide frequency band.
A possible alternative is the use of negative capacitance circuits. Park[7] developed a shunting strategy based on

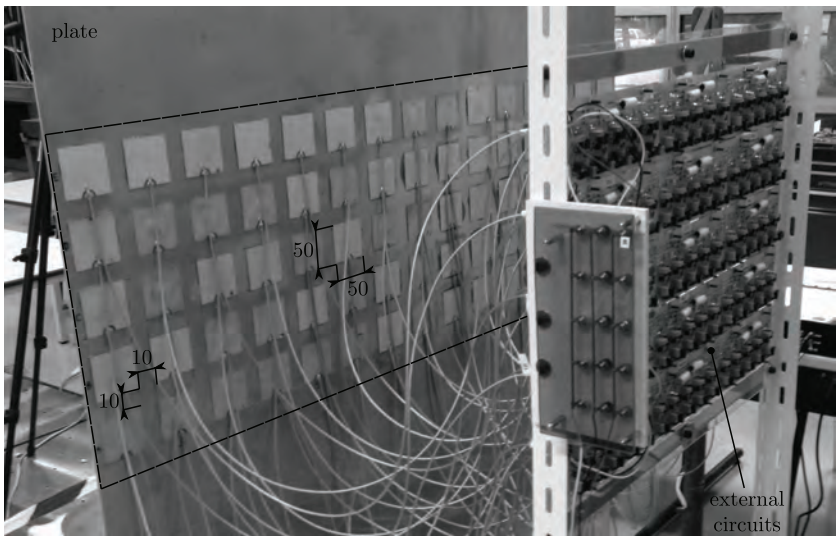

Figure 1. plate with 75 element piezoelectric patch array comprising an active interface, connected to bank of 75 individual negative impedance shunt control circuits. Patch dimensions and spacing annotated on photograph.

a fixed negative capacitance circuit with the objective of simplifying the electrical network.
In this paper, an array of piezoelectric patches shunted to a set of negative capacitance circuits and periodically arranged over a limited region of the surface of a two-dimensional waveguide is considered. This array of patches is intended to serve as an active interface between regions of the waveguide, formed from a plate. This active interface allows modification of the scattering properties of the waveguide in terms of reflected and absorbed energy. This controlling capability is obtained by correctly tuning the parameters of the external circuit by which almost arbitrary effective structural impedance may be obtained. The selection of the electric component is made according to the methodologies developed by Collet.[8]
A finite element-based design methodology is used to predict the attenuation properties of the smart structure. The predictions are then experimentally validated by measuring the harmonic response of the plate and evaluating some derived quantity such as the loss factor and the kinetic energy ratio. The loss factor and the kinetic energy ratio (calculated in each subdomain of the plate) are used to qualify the absorbing and reflecting properties of the metacomposite. The validated model is also used to explore different configurations with the aim of defining some general design criteria and then assess the robustness of the overall system.
The remainder of this paper is organized into four sections. The first section provides a review of the design of the plate, piezoelectric array, and shunt circuits for the control system applied to the patches in the piezoelectric array. The second section describes the numerical model used to investigate the system. The third section presents the experimental and numerical results. Finally, the last section summarizes the major findings presented in this paper and provides recommendations for future investigation.

2. METACOMPOSITE DESIGN

The basic structure of the metacomposite comprises an aluminum plate and array of piezoelectric patches as depicted in Figure 1. The plate is suspended from a rigid frame by metallic wires in order to approximate free-free boundary conditions. The plate ($2100 \times 1050\ mm^2$) is equipped with 75 piezoelectric patches (Ferroperm Industries PZ 26 series) arranged in a regular 15×5 array. The system's configuration depicted in Figure 1 is associated to the label A, along the paper other configuration are also studied by modifying some geometrical parameter as summarized in Table 1. The parameter L_{pz} l_{pz} and h_{pz} represent respectively the length of the piezoelectric ceramic along the x, y and z axes; p_x and p_y symbolize the distance between two adjacent piezoelectric ceramic in x and y direction; L_{int} and l_{int} are associated to the extension of the active interface.
The length and the depth of the patch array were selected based on consideration of their size relative to the shortest structural wavelength of interest. The array was intended to be effective up to a frequency of 5000

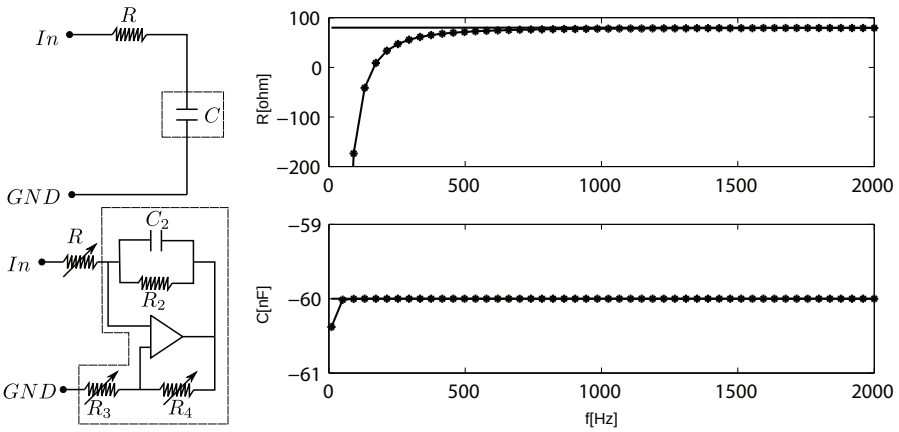

Figure 2. Ideal vs. real-life circuit. On the left the basic architecture for both circuits is presented. On the right the circuit's impedance is depicted in terms of equivalent resistance (top) and equivalent capacitance (bottom): the solid line represent the ideal circuit; the solid line with markers the real-life circuit.

Hz. The plate's dispersion relation for the A_0 flexural mode at 5000 Hz has a wavelength of approximately 30 cm. With patches having dimensions of 50×50 mm, there will be no charge cancellation on an individual patch as would occur if the patch dimensions were comparable to a wavelength. Further, the depth of the patch array is 350 mm such that it spans more than a wavelength at 5000 Hz. Since the array elements are uncoupled electronically, each element within the array would still function at the highest frequency of interest, even though the entire array depth would be comparable to a wavelength.

The thickness of the patch was selected considering the constraints of the electric circuit and the nature of the control technique. Different authors have shown that the best controlling effect is obtained when the negative impedance shut circuit is tuned close to the inherent patch capacitance (Livet[10]). This property strongly depends on the material properties and the geometry of the patch. Once the material properties and the two dimensions of the piezoelectric patch are chosen, the only parameter which remains for selection is the thickness. Thin patches exhibit larger values of intrinsic capacitance which would yield increased control, however, this parameter cannot be reduced indefinitely due to the weakening of the piezoelectric patch itself. For these reasons, a thickness of 0.5 mm was selected.

The results presented in Collet[8] provide an approach for optimization of the external shunt circuit in terms of the real and the imaginary parts of the synthetic impedance. The authors identified two possible behaviors depending on the criterion used in the optimization. The first one is the minimization of the velocity of the energy propagation in the region of the active array which limits the propagation of the waves beyond the active interface.

As an alternative, by choosing a criterion based on the maximization of the electrical damping it is possible to modify the dynamic properties of the plate by increasing the energy absorption properties of the active interface. Optimization of the electric synthetic impedance parameters for this criterion leads to design of an absorbing metacomposite able to reduce the vibratory energy flowing through it by increasing the power dissipated within the electric circuit. This optimal case requires a negative capacitance and a positive and larger frequency-dependent resistance as compared to the reactive interface criterion described above.

For the work presented here, the layout of the actual circuit implemented for control of the patches is presented

type	patch #	L_{pz}	l_{pz}	h_{pz}	p_x	p_y	L_{int}	l_{int}
A	15×5	50	50	0.5	10	10	1050	850
B	15×5	50	150	0.5	10	10	1050	350
C	20×7	50	30	0.5	10	10	1050	350

Table 1. Smart interface's configurations and piezoelectric ceramic's dimensions expressed in mm.

in Figure 2. This circuit contains a number of passive components, including the resistances R , R_2 , R_3 , R_4 and the capacitance C_2, as well as an active component, specifically, an operational amplifier that is essential for the circuit to reproduce the desired negative capacitance behavior. This specific circuit layout was chosen as opposed to others (Fleming[11]) because of its simplicity and its effectiveness in the frequency range of interest. The impedance of the circuit in Figure 2 is determined by the formula

$$Z_{eq}(\omega) = R_{eq} + \frac{1}{i\omega C_{eq}} = R - \frac{R_3 R_2}{R_4(1 + i\omega R_2 C_2)}. \tag{1}$$

Figure 2 depicts the frequency-dependent behavior of the actual impedance produced by the real-life circuit; in the upper part of Figure 2 the equivalent resistance R_{eq} is compared to the ideal resistance R and at the bottom the equivalent capacitance C_{eq} is compared to the ideal capacitance C. Both terms vary as a function of the frequency; in particular the resistance at low frequency presents a negative value that can introduce some instability which can degrade the overall performance of the control system and it is compensated by a positive input resistance R. For relatively high frequency values, the equivalent resistance R_{eq} and the equivalent capacitance C_{eq} are modified according to the following formulae

$$R_{eq} = R, \quad C_{eq} = C_{neg} = -\frac{R_4}{R_3} C_2. \tag{2}$$

The negative impedance control technique requires tuning of the synthetic capacitance around the capacitance value of the piezoelectric ceramic at free stress condition; this value is intrinsic to the electromechanical coupling and depends upon the material properties, the geometry of the patches and the plate stiffness. The intrinsic capacitance of the piezoelectric patch can be estimated by measurement using a capacitance meter when the specimen is free of external forces. In the present case the measured nominal patch capacitance is 50 nF. The actual circuit was tuned by varying the ratio R_4/R_3 in small increments from high negative values of the synthetic capacitance to a value very close to the targeted intrinsic capacitance value.
For the work at hand, two configurations of the of circuit have been implemented in order to program two different vibroacoustic behaviors:

- Case 1 corresponding to a lightly-damped, reflective configuration. It is obtained by tuning the negative capacitance C_{neg} very close to the instability point of the piezoelectric ($C_{neg} = -52$ nF). The input resistance R is set to a small positive value able to reproduce the desired behavior (wave reflection) and still ensuring the stability of the control system ($R = 40$ Ω).
- Case 2 corresponding to an absorbing configuration. It is obtained by tuning the negative capacitance C_{neg} with the same value of Case 1 ($C_{neg} = -52$ nF). The energy absorption enhancement is then obtained by imposing a larger input resistance ($R = 400$ Ω).

3. NUMERICAL MODEL

Consider the flexible piezoelectric structure depicted in Figure 3 occupying the volume V_s and subjected to a prescribed displacement $\bar{u}$ on a part S_u and to surface force distribution f on the complementary part S_f of its external boundary. Let n be the unit normal external to V_s. The electric boundary conditions are defined by a prescribed surface charge $\bar{q}$ on S_q and an electric potential $\bar{\phi}$ on the remaining part S_ϕ. The local set of equilibrium equations describing the mechanical and the electrical domain are given by

$$\begin{aligned} \rho\ddot{u} - \nabla \cdot \sigma &= f \\ \nabla \cdot D &= 0 \end{aligned} \tag{3}$$

where u is the displacement field, σ is the symmetric Cauchy stress tensor, D denotes the electric displacement vector components and ρ is the mass density of the structure. The differential problem is defined once the boundary conditions are defined

$$\begin{aligned} &\sigma \cdot n = T && \text{on } S_f \\ &u = \bar{u} && \text{on } S_u \\ &D \cdot n = -\bar{q} && \text{on } S_q \\ &\phi = \bar{\phi} && \text{on } S_\phi \end{aligned} \tag{4}$$

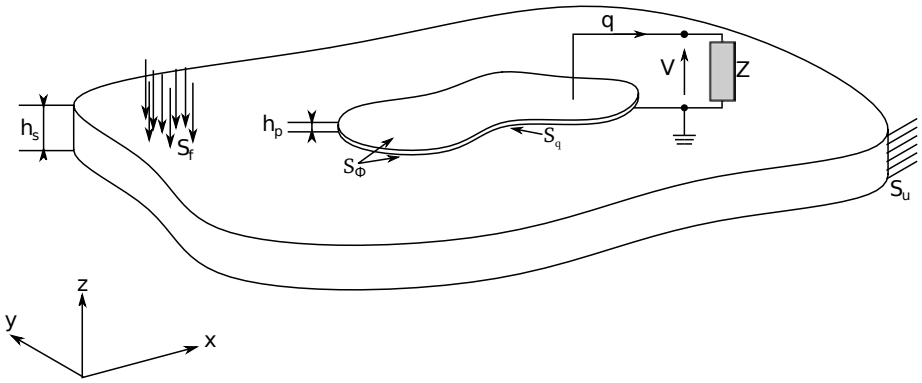

Figure 3. Plate with arbitrarily shaped piezoelectric ceramic shunted to an electric impedance.

where T indicates the component of the stress tensor projected along the outpointing normal, $\bar{u}$ the imposed displacement, $\bar{q}$ the imposed charge and $\bar{\phi}$ the imposed voltage.
The stress tensor and electric displacement are related to the linear strain tensor ε and electric field E through the constitutive laws for a piezoelectric material (Royer[12])

$$\begin{aligned} \sigma &= C_E \varepsilon - e^T E \\ D &= e\varepsilon + \epsilon_S E \end{aligned} \tag{5}$$

where C_E, e, ϵ_S denote the mechanical stiffness matrix evaluated at constant electric field, the piezoelectric stress coupling matrix and the permittivity matrix at constant strain, respectively.
The strain tensor is calculated as

$$\varepsilon = \nabla_s u = \frac{1}{2}\left(\nabla u + \nabla^T u\right), \tag{6}$$

while the electric field and the voltage are related through the simple formula

$$E = -\nabla\phi. \tag{7}$$

Within a finite element framework, the field variables u and ϕ are related to nodal degrees of freedom d and V through a proper selection of shape functions N_u and N_ϕ

$$u = N_u d \quad \phi = N_\phi V. \tag{8}$$

By assuming an harmonic motion at frequency ω for each variable the following electro-elastic system of equations is obtained

$$\begin{aligned} K_{uu}\hat{d} + K_{u\phi}\hat{V} - \omega^2 M_{uu}\hat{d} &= \hat{f} \\ K_{\phi u}\hat{d} + K_{\phi\phi}\hat{V} &= \hat{q} \end{aligned} \tag{9}$$

the symbol $\hat{}$ over each physical quantity denotes its complex amplitude in the frequency domain.
The combination of the host structure and the piezoelectric patches is modeled using 4-node Kirchhoff plate elements (Hughes[13]), the electric field is assumed to be constant on the surface of each piezoelectric patch and the electric potential is assumed to vary linearly through the thickness.
Under these assumptions, the electrical equation can be reduced to the form

$$K_{\phi u}\hat{d} + K_{\phi\phi}\hat{V}_p = \hat{q}. \tag{10}$$

Application of the shunting circuit to the electrodes of the piezoelectric patch allows condensing out equations (9) to obtain

$$\left(K_{uu} - \omega^2 M_{uu} + S_{uu}\right)\hat{d} = \hat{f} \tag{11}$$

where S_{uu} is the shunting matrix describing the effect of the shunting circuits on the dynamic behavior of the structure. It is given by

$$S_{uu} = j\omega K_{u\phi} \left(j\omega K_{\phi\phi} - K_Z \right)^{-1} K_{\phi u} \tag{12}$$

where $K_{\phi\phi}$ is the matrix containing the terms related to the intrinsic capacitance C_p and K_Z is the matrix containing the terms related to the impedance Z of the shunting circuit in Figure 3. The impedance of each piezoelectric ceramic establishes a relation between the voltage $\hat{V}$ and the flowing charge $\hat{q}$ according to the following equation

$$\hat{V} = Zj\omega\hat{q}. \tag{13}$$

It is clear that the shunting matrix can affect the inertial, the damping or the stiffness properties of the structure depending on the characteristic of the piezoelectric patch and the shunting circuit parameters contained in the impedance Z.

To better understand the underlying physics of this control system an energy balance analysis including time-varying quantities such as velocities and forces has been conducted. Equation (11) represents a linear n-DOF mechanical system vibrating harmonically under the action of an external force.
The main goal of this section is to recall some equations relating various energy characteristics such as the power flow, the kinetic energy and others. Under an harmonic excitation each of these quantities can be represented as the sum of three harmonically varying components, as an example let us consider the power flow

$$\mathcal{P}(t) = F(t) \cdot v(t) = P_0 + P_c \cos 2\omega t + P_s \sin 2\omega t. \tag{14}$$

where $F(t)$ and $v(t)$ are the time histories of the force and the velocity associated to a point belonging to the domain. The three components in equation (14) are independent in the sense that they are orthogonal in the time interval $2\pi/\omega$.
The terms P_0, P_c and P_s can be easily estimated using the complex numbers formalism, for example the alternating components of $\mathcal{P}$ in the frequency domain is simply the product of the complex amplitude of the velocity and the force

$$P = v^T F = P_c + jP_s. \tag{15}$$

likewise the continuous components are calculated as the product of the force and the conjugate of the velocity

$$P^* = v^{*T} F = P_0 + jP_q. \tag{16}$$

The term P_q is not related to any significant physical quantity but rather represents the part of the velocity vector in quadrature with the external force.
Other quadratic quantities such as the kinetic and the potential energy are represented in a similar manner. However, unlike the power flow, they all have zero reacting component. For example we can consider the kinetic energy

$$\begin{aligned} T &= \frac{1}{4} v^T M v = T_c + jT_s \\ T^* &= \frac{1}{4} v^{*T} M v = T_0 \end{aligned} \tag{17}$$

the sum of the kinetic energy T_0 and the potential energy W_0 determines the total energy E_0 of the system

$$E_0 = W_0 + T_0 \tag{18}$$

All these quantities allows one to qualify the performances of the control system. For example by calculating the active power flow P_0 and the total energy E_0 it is possible to estimate the loss factor η of the structure (Bobrovnitskii[14]) by simply calculating

$$\eta = \frac{P_0}{\omega E_0}. \tag{19}$$

Another important quantity able to quantify the amount of kinetic energy confined in a specific portion of the plate is kinetic energy ratio τ

$$\tau = \frac{T_0^i}{T_0^{tot}}. \tag{20}$$

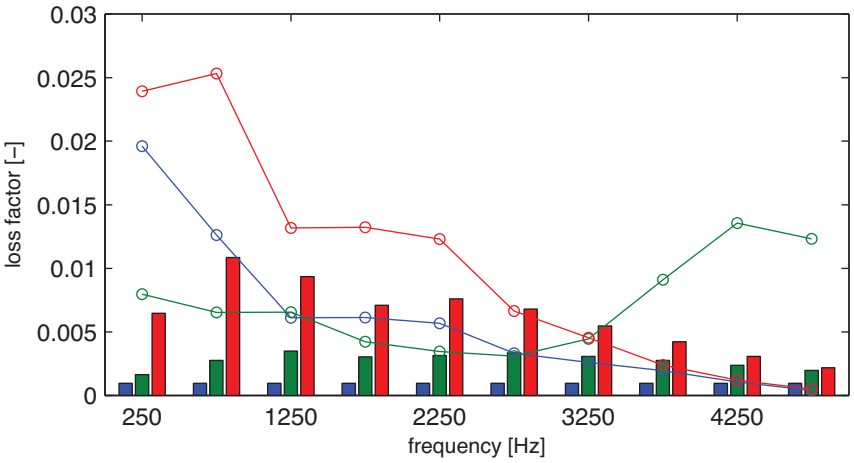

Figure 4. Loss factor of the smart plate, the lines represent the experimental data and the bars the calculated solutions. The color code indicates: the uncontrolled plate (blue), controlled plate with $R = 40\ \Omega$ (green) and $R = 400\ \Omega$ (red).

where T_0^{tot} represents the sum of three constituting regions of plate plate, namely the lower and the upper region and the interface.

4. RESULTS

4.1 Harmonic Response of the Metacomposite

A periodic lay-out of 15×5 piezoelectric patches is placed on the top surface of the host structure, 850 mm away from the lower side. The plate is excited by a point force located in the lower left corner of the plate, the response is evaluated in terms of out-of-plane velocity calculated at the opposite corner and its derived quantities such as the loss factor and the kinetic energy ratio. The FE mesh features 46×70 rectangular plate elements.
In Figure 4 the calculated and the measured loss factors are compared in three different conditions: open circuit, negative capacitance control strategy with $R = 40\ \Omega$ and $R = 400\ \Omega$. In Figure 4 the lines are associated to the experimental measurements while the bars are associated to the calculated solutions. The blue items represent the baseline solution, by comparison it is clear that the calculated solution underestimate the total amount of dissipated energy. For example is not easy to include in the considered model the dissipation mechanism associated to the friction of the electric wires with the plate's surface (Figure 1). Another neglected source of dissipation is the external electric circuit, in the theoretical model each circuit is assumed to be open but this is not the case since each circuit is still connected to the external circuit in absence of power. Under these conditions the circuit is not able to reproduce the negative capacitance effect but it is reasonable to assume that each circuit can still add an extra amount of damping due to the current flowing within the circuit.
In Figure 5 the calculated and measured kinetic energy ratio is compared in three different conditions: open circuit, negative capacitance control strategy with $R = 40\ \Omega$ and $R = 400\ \Omega$. The results are collected in three different diagrams representing respectively the ratio of kinetic energy confined in the upper portion of the plate, within the plate and in the lower portion of the plate. If we consider the part of the plate under the smart interface larger values of the kinetic energy ratio are associated to an increase of kinetic energy in the considered area. Under these conditions the vibrating field is modified, the smart interface is capable to confine the kinetic energy in a specific portion of the plate. The energy confined in the lower portion of the plate increases from 1250 to 3250 Hz for the absorbing configuration and then is shifted toward higher frequencies decreasing the input resistance. Beyond 2500 Hz the reflecting configuration provide better performances; the active interface acts like an electro-mechanical filter that prevents the occurrence of the standing-waves. The obtained results are in good agreement with the experimental measurements even if the theoretical results constantly overestimate the confined energy.

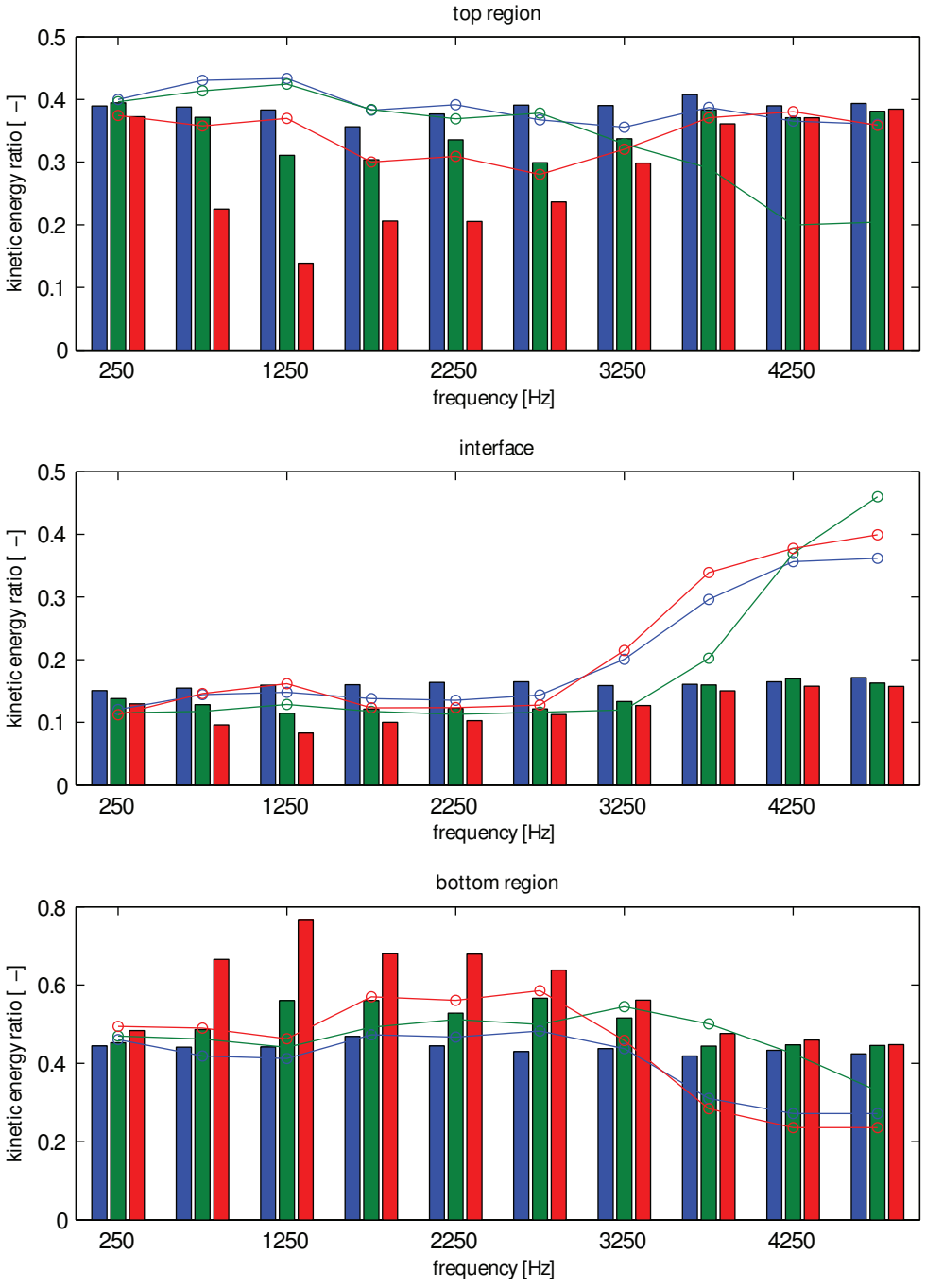

Figure 5. Kinetic energy distribution of the smart plate, the lines represent the experimental data and the bars the calculated solutions. The color code indicates: the uncontrolled plate (blue), controlled plate with $R = 40\ \Omega$ (green) and $R = 400\ \Omega$ (red).

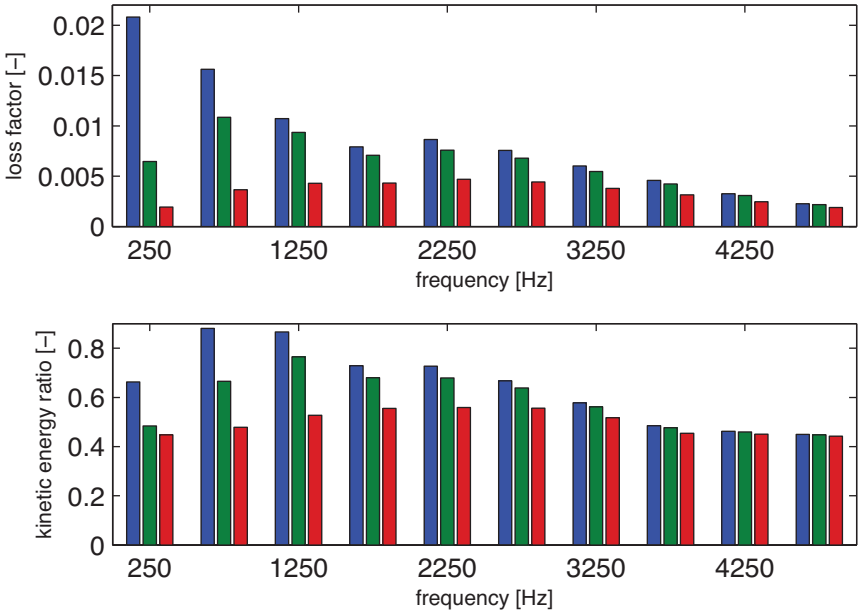

Figure 6. Loss factor and lower region's kinetic energy distribution of the smart plate for different value of negative capacitance. The blue bars indicates the controlled plate $C_{neg} = -51.3\ nF$; the green bars the controlled plate $C_{neg} = -55.7\ nF$ and red bars the controlled plate $C_{neg} = -59\ nF$. In all cases a resistance of $R = 400\ \Omega$ has been chosen.

4.2 The Effect of the Circuit's Parameters

The performances of the control system can be improved by properly tuning the external circuit. In order to highlight this dependency a parametric analysis has been performed considering a variation of the negative capacitance.

In Figure 6 the loss factor of the controlled structure is compared to the reference solution for three different values of negative capacitance. The blue bars are associated to a negative capacitance of 51.3 nF while the green and the red bars represent a negative capacitance of 55.7 and 59 nF respectively.

As expected the performances of the system degrade as one move away from the point corresponding to the opposite of the intrinsic capacitance C_p. An interesting feature is the fact that larger attenuation is obtained for $C_{neg} = 51.3\ nF$ over a narrower frequency band, namely $0 - 1000\ Hz$ whereas for a bigger value of negative capacitance the overall performances are slightly reduced but broadened up to 5000 Hz. The filtering properties of the smart interface are enhanced introducing a negative capacitance control system. In particular with negative capacitance values closed to C_p the system is able to increase this indicator up to 0.8 in the 1000 Hz frequency band (Figure 6). The red bar representing the largest considered value of negative capacitance still shows acceptable performances, this fact can be used as illustration of the robustness of the proposed system.

The circuit's model can be further refined by considering the actual impedance as presented in equation (1). The layout of the actual circuit includes an operational amplifier employed as a gyrator. This specific circuit architecture originates a negative resistance at low frequencies that determine an energy increase detrimental for the system's stability as shown in the equation of the real-life impedance.

This effect is clearly observed in Figure 7 where the experimental loss factor in the 250 Hz frequency band assumes the value of 0.025, it increases up to almost 0.03 and then decreases when the excitation frequency is increased. This trend is better observed for the real life circuit represented by the blue bars, in this case the loss factor is decreased at low frequencies. At higher frequency values no differences between the two mathematical models are observed. This last observation suggests that in most of the cases the former approach can be used without loss of reliability. We should point out that both approaches lack of some prediction capabilities due to the fact that is not easy to take into account each aspect of the real-life circuit in particular the actual behavior of the operational amplifier and the contribution of the auxiliary circuit introduced in order to detect the occurring instability (LED circuit).

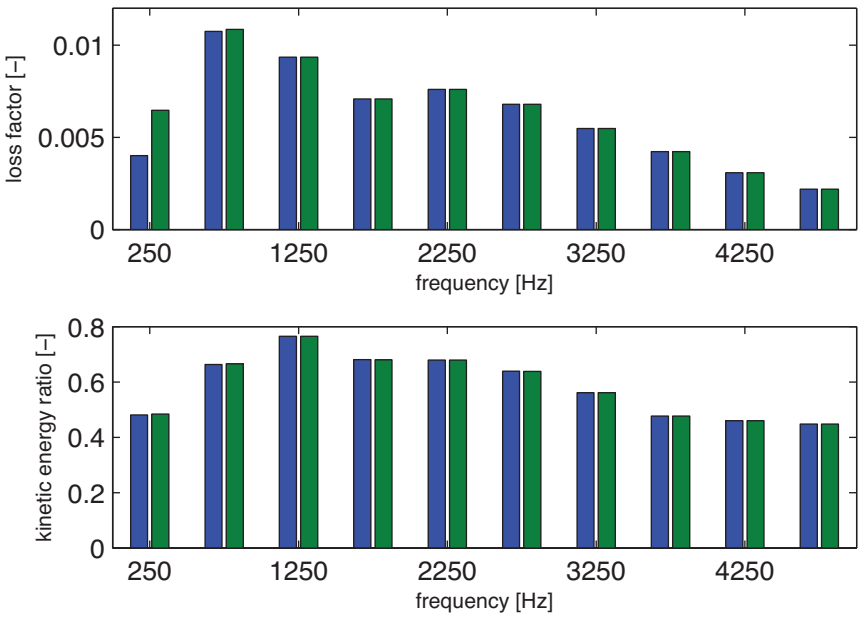

Figure 7. Loss factor and lower region's kinetic energy distribution of the smart plate for different circuit layout. The blue bars indicate the controlled plate with real-life circuit and the green bars the ideal circuit with an input resistance of $R = 400\ \Omega$. The parameters of the real-life circuit have been chosen in order to reproduce the same capacitance at higher frequencies.

Regarding the kinetic energy distribution (Figure 7) the two models give the same results showing that the enhanced circuit model has an effect on the active part of the impedance leaving unchanged the reactive ones.

4.3 Smart Interface Acting Like a Robust Frequency Filter

The section's main objective is to show how the control system acts as a filter capable of suppress vibrations in a specific frequency band. To do so the topology of the smart interface has been analyzed, by variating the geometry of the piezoelectric actuators or the layout of the smart interface is possible to modify the behavior of the control system.
These mechanisms have been analyzed by considering two different interface's layouts presenting an array of 15×5 (interface type B) and 20×7 (interface type C) piezoelectric actuators respectively and for each of which different ceramics' dimensions have been considered, see Table 1.
In Figure 8 the structure's loss factor is compared for the two different interface layout. The blue bar associated to the configuration 15×5 shows higher loss factor values at very low frequencies, in the 250 Hz frequency band the averaged loss factor exceeds the value of 0.02 for higher values a deterioration in performance is observed in particular beyond 1000 Hz the 15×5 configuration appears less effective than configuration 20×7 (green bar). Configuration 20×7 provides good performances from 1000 to 10000 Hz. Moreover, respect to configuration 15×5 the value of the loss factor decrease less dramatically from one band to another, for instance a value of almost 0.01 is preserved over a frequency range of almost 5000 Hz. According to these results it is clear that the dimensions of the smart interface have a large impact on the performance of the control system.
As a rule of thumb the length of the piezoelectric actuator should respect the following condition

$$L < \frac{\lambda^*}{2} \tag{21}$$

where λ^* represent the wavelength of the targeted mode. For example examining the dispersion relation of the A_0 mode of the bare plate at 10000 Hz one obtains a wavenumber $k^* = 120\ rad/m$ and a wavelength $\lambda^* = 5.2$ cm, this means that the maximum length of the ceramic will be less than 2.6 cm. This result is in good agreement with the calculated response. A 3 cm long ceramic is not able to exert any appreciable control in this specific

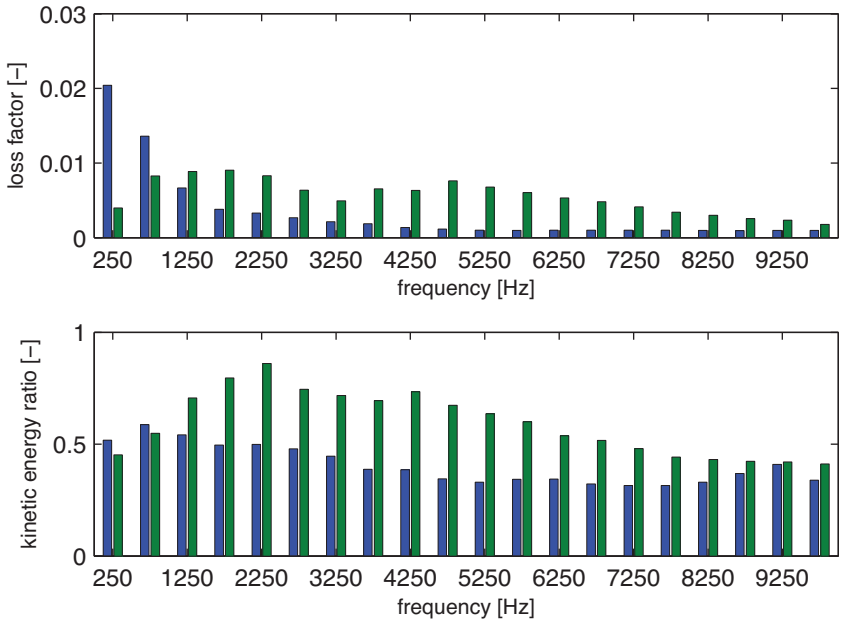

Figure 8. Loss factor and lower region's kinetic energy distribution of the smart plate for different interface topologies. The blue bars indicate the controlled plate with type B interface and the green bars the controlled plate with type C interface. In both cases an input resistance of $R = 400\ \Omega$ has been selected.

frequency band.

Similar considerations can be done about the averaged kinetic energy distribution within the plate. Configuration 15×5 represented by blue bars in Figure 8 shows that the energy is evenly spread in the bottom part of the plate, there is not preferred frequency band, even if at very low frequencies the active interface seems to better filter the vibrating field increasing the ratio up to 0.6. Interface type B represented by green bars in Figure 8 behaves in a better way, in the $250 - 8250\ Hz$ the energy ratio is increased from 0.5 to 0.8.

5. CONCLUSIONS

A periodic configuration of negative capacitance shunted piezoelectric patches is used to control vibrations of a freely suspended aluminum plate.

Numerical investigations shown that the tuning capabilities of the negative capacitance networks can be effectively used to obtain a broadband control effect. The behavior of the smart plate is characterized by two different control mechanisms: the negative capacitance branch eliminates the parasitic effect due to the intrinsic capacitance of the piezoelectric ceramic enhancing the attenuation capabilities of the smart structure and the periodic lattice of piezoelectric actuator selectively filters the incident waves preventing the energy to pass through the smart interface.

The validated model allows to define some design criteria such as the choice of the electrical components, the size and the shape of the periodic lattice of piezoelectric patches.

ACKNOWLEDGMENTS

This study is a collaborative effort supported by the French Research Agency under grant number NT09-617542 (CALIOP Project) and ANR-11-LABX-0001-01 (Labex Action).

REFERENCES

1. R. Forward, "Electronic damping of vibrations in optical structures," *Applied Optics* **18**(5), pp. 690–697, 1979.
2. N. Hagood and A. von Flotow, "Damping of structural vibrations with piezoelectric materials and passive electrical networks," *Journal of Sound and Vibration* **146**(2), pp. 243–268, 1991.
3. S. Wu, "Multiple PZT transducers implemented with multiple-mode piezoelectric shunting for passive vibration damping," in *Proc. SPIE 3672, Smart Structures and Materials*, pp. 112–122, 1999.
4. J. Hollkamp, "Multimodal passive vibration suppression with piezoelectric materials and resonant shunts," *Journal of Intelligent Material Systems and Structures* **5**(1), pp. 49–57, 1994.
5. O. Thorp, M. Ruzzene, and A. Baz, "Attenuation of wave propagation in fluid-loaded shells with periodic shunted piezoelectric rings," *Smart Materials and Structures* **14**(4), p. 594, 2005.
6. A. Spadoni, M. Ruzzene, and K. Cunefare, "Vibration and wave propagation control of plates with periodic arrays of shunted piezoelectric patches," *Journal of Intelligent Material Systems and Structures* **20**(8), pp. 979–990, 2009.
7. J. Park and D. Palumbo, "A new approach to identify optimal properties of shunting elements for maximum damping of structural vibration using piezoelectric patches," in *Proc. Active 2004 conference*, 2004.
8. M. Collet, M. Ouisse, and M. Ichchou, "Structural energy flow optimization through adaptive shunted piezoelectric metacomposites," *Journal of Intelligent Material Systems and Structures* **23**(15), pp. 1661–1677, 2012.
9. M. Collet, M. Ouisse, M. Ichchou, and R. Ohayon, "Semi-active optimization of 2D wave dispersion into shunted piezo-composite systems for controlling acoustic interaction," *Smart Materials and Structures* **21**(9), p. 94, 2012.
10. S. Livet, M. Collet, M. Berthillier, J. Pierrick, and J. Cote, "Structural multi-modal damping by optimizing shunted piezoelectric transducers," *European Journal of Computational Mechanics* **20**(1-4), pp. 73–102, 2011.
11. A. Fleming, S. Behrens, and S. Moheimani, "Synthetic impedance for implementation of piezoelectric shunt-damping circuits," *Electronics Letters* **36**(18), pp. 1525–1526, 2000.
12. D. Royer and E. Dieulesaint, *Elastic waves in solids*, Springer, 2000.
13. T. Hughes, *The finite element method linear static and dynamic finite element analysis*, Dover Publications, 2000.
14. Y. Bobrovnitskii, "Conservation laws in vibration theory," *Doklady Physics* **49**(3), pp. 171–174, 2004.